EUROPEAN ORGANIZATION FOR NUCLEAR RESEARCH

CERN/EP 86-6
6 January 1986

NEUTRAL AND CHARGED D^* PRODUCTION IN 360 GeV/c $\pi^- p$ INTERACTIONS

LEBC-EHS Collaboration

Aachen[1], Bombay[2], Brussels[3], CERN[4], College de France[5], Genova[6], Japan Universities[7] (Chuo University, Tokyo Metropolitan University, Tokyo University of Agriculture and Technology), Liverpool[8], Madrid[9], Mons[10], Oxford[11], Padova[12], Paris[13], Rome[14], Rutherford[15], Rutgers[16], Serpukhov[17], Stockholm[18], Strasbourg[19], Tennessee[20], Torino[21], Trieste[22] and Vienna[23]

M. Aguilar-Benitez[9], W.W. Allison[11], J.F. Baland[10], S. Banerjee[2], W. Bartl[23], M. Begalli[1], P. Belliere[5], A. Bettini[12], L. de Billy[13], R. Bizzarri[14], G. Borreani[21], H. Briand[13], R. Brun[4], W.M. Bugg[20], E. di Capua[14], C. Caso[6], B. Castano[9], E. Castelli[22], P. Checchia[12], P. Chilapnikov[17], S. Colwill[11], R. Contri[6], D. Crennell[15], M. Cresti[12], A. De Angelis[12], C. Defoix[5], R. Dimarco[16], J. Dolbeau[5], J. Dumarchez[13], B. Epp[23], S. Falciano[14], C. Fernandez[4], C. Fisher[15], Y. Fisyak[17], F. Fontanelli[6], J.R. Fry[8], S. Ganguli[2], L. Garbellini[21], U. Gasparini[12], S. Gentile[14], A. Goshaw[4], F. Grard[10], A. Gurtu[4], R. Hamatsu[7], T. Handler[20], E.L. Hart[20], L. Haupt[18], S. Hellman[18], J.J. Hernandez[4], S.O. Holmgren[18], M.A. Houlden[8], J. Hrubec[23], P. Hughes[15], D. Huss[19], Y. Iga[7], M. Iori[14], E. Jegham[19], E. Johanson[18], J. Kesteman[10], E. Kistenev[17], I. Kita[7], S. Kitamura[7], V. Kniazev[17], P. Ladron de Guevara[9], M. Laloum[5], J. Lemonne[3], H. Leutz[4], L. Lyons[11], M. MacDermott[15], P.K. Malhotra[2], F. Marchetto[21], G. Marel[14], F. Marzano[14], M. Mazzucato[12], A. Michalon[19], M.E. Michalon-Mentzer[19], T. Moa[18], R. Monge[6], L. Montanet[4], G. Neuhofer[4], H.K. Nguyen[13], S. Nilsson[18], H. Nowak[4], N. Oshima[7], G. Otter[1], G.D. Patel[8], M. Pernicka[23], P. Pilette[10], C. Pinori[12], G. Piredda[14], R. Plano[16], A. Poppleton[4], P. Poropat[22], B. Powell[4], G. Ransone[1], M. Regler[23], S. Reucroft[4], J. Richardson[4], K. Roberts[8], H. Rohringer[23], M. Schouten[4], R. Schulte[1], B. Sellden[18], M. Sessa[22], K. Shankar[2], S. Squarcia[6], P. Stamer[16], V. Stopchenko[17], W. Struczinski[1], A. Subramanian[2], M.C. Touboul[13], U. Trevisan[6], C. Troncon[22], T. Tsurugai[7], V. Uvarov[17], L. Ventura[12], P. Vilain[3], E. Vlasov[17], C. Voltolini[19], B. Vonck[3], B.M. Whyman[8], J. Wickens[3], C. Willmott[9], P. Wright[11], T. Yamagata[7], P.L. Zotto[12] and G. Zumerle[12]

Submitted to Physics Letters B

EP/2732P/SR/mk

During the last few years some progress has been made in the understanding of charm meson hadroproduction. The experimental information, however, relies almost entirely on D studies, while very little is known about the production of excited states. In particular, the relative importance of D and D^* in hadroproduction(*), essential for the understanding of fragmentation and recombination processes, is only poorly known. What knowledge there is derives from data obtained in a limited Feynman x region and therefore suffers from large acceptance corrections [1].

In this letter we report on the properties of both neutral and charged D^* mesons, produced in the reaction $\pi^- p \to D^* + X$, at a beam momentum of 360 GeV/c. Data were collected at the CERN SPS, using the LExan Bubble Chamber (LEBC) as vertex detector, associated with the European Hybrid Spectrometer (EHS), for which there is good acceptance in the whole positive x_F hemisphere. The details of the experimental apparatus are given in ref. [2] and will not be repeated here.

In previous publications [3] and [4] we have discussed the production properties of charm D^0 and $D^\pm$ mesons and presented evidence for leading particle effects. In the earlier experiment however [3] we could not extract significant D^* production properties, due to low statistics and to the presence of kinematical ambiguities. In addition to an increased sensitivity of 15.8 ev/μb, the present experiment [4] has decisively better vertex resolution, with resolved bubble diameter of $\leq$ 20 μm and much improved particle identification [5]. This allows a qualitative change in the understanding of the charm events, in particular in the resolution of ambiguities between different charm decay hypotheses.

(*) We write D^0 for $D^0/\bar{D}^0$ and D^* for $D^*/\bar{D}^*$ unless otherwise indicated.

The search for D^* is based on the 57 reconstructed D decays with $x_F > 0.0$ (*) discussed in an earlier publication [2]. Details of the scanning, measuring and geometrical reconstruction of the events, as well as the selection criteria used to extract the final charm sample are given in [2] and in [4]. The 57 decay sample consists of 35 neutral and 22 charged D mesons. Within this sample, 8 decays are $D^o/\bar{D}^o$ ambiguous while for 27 decays the particle or antiparticle nature of the D^o is unambiguously determined. We stress here that the D selection is based on the decay final state and consequently is not biased against or in favour of D^* production.

The full line histogram of fig. 1 shows the combined $D^o\pi^+$ and $\bar{D}^o\pi^-$ effective mass spectrum. For the 8 ambiguous $D^o/\bar{D}^o$ decays, both positive and negative primary pions are considered for the invariant mass combinations. The shaded area represents the background evaluation described below. A narrow peak at threshold is clearly visible. This peak is attributed to the $D^*(2010)$ resonance. The width of the peak is determined by our experimental resolution of 10 MeV FWHM, as shown by the solid line in fig. 1. Of the 10 entries in the D^* region, 5 lead to D^o decaying to four charged particle (V4) and 5 to two charged particle (V2) topologies, respectively.

To evaluate the background below the D^* signal, we used a sample of 49 decays, the 27 unambiguous D^o decays for which the "wrong" mass combinations $M(D^o\pi^-)$ and $M(\bar{D}^o\pi^+)$ can be defined and the 22 $D^\pm$ decays with unique fits, for which we do not expect a D^* signal in the $D^\pm\pi^\mp$ effective mass. To avoid the slightly different thresholds between the $D^\pm\pi^\mp$ and $D^o\pi^\pm$ systems we attribute the D^o mass to the $D^\pm$ when we compute the $D^\pm\pi^\mp$ effective mass.

(*) Applying the x_F cut to D^o is equivalent to making the same cut to D^*, given the small Q value of the $D^* \to D\pi$ decay.

The distribution of these effective masses, normalized to the number of entries with $M(D^{o}\pi^{\pm}) > 2.015$ GeV/c, is shown in fig. 1 as a shaded histogram. From this, we estimate the possible background contribution to the D^{*} signal to be approximately 1.5 events. This is also confirmed by a Monte-Carlo simulation, shown in the figure as a broken line.

In summary, therefore, we observe a D^{*} signal of 8.5 entries on a background of 1.5. This is from a full sample of 35 D decays. The ratio R_1 of $D^{*\pm}$, decaying into $D^{o}\pi^{\pm}$ to the total number of D^{o} with $x_F > 0.0$ is found to be:

$$R_1 = \frac{\sigma(D^{*\pm} \rightarrow D^{o}\pi^{\pm})}{\sigma(D^{o})} = 0.24 \,^{+0.09}_{-0.06} \quad .$$

We have used two additional approaches, which do not rely on kinematic fits and consequently use a larger number of the neutral charm decays, to further investigate D^{*} production. This larger D^{o} sample consists of 15 V4 and 45 V2 decays having at least two tracks reconstructed in the spectrometer with a total longitudinal momentum greater than 16 GeV/c. These requirements remove the events in the negative x_F region. Any possible contamination in the V2 charm events from gamma conversion and strange particle decays has been eliminated by requiring that the opening angle is seen to be non-zero in the bubble chamber and that at least one of the tracks has a $p_T > 250$ MeV/c, relative to the line-of-flight of the parent particle [2].

The first method is based on the fact that the small Q-value of the D^{*} meson decay into the $D\pi$ channel constrains the p_T of the decay π, relative to the D line-of-flight, to be less than 42 MeV/c (the mean measurement errors are of the order of 15 MeV/c). Therefore, we should see a D^{*} signal as an excess of events at low p_T values. The p_T distribution of the primary pions, relative to the D^{o} line-of-flight, is shown in fig. 2(a). In this histogram, for each decay, only the smallest value is plotted, to reduce the combinatorial background without introducing a loss in the D^{*} signal. The shaded area is the same distribution for uncorrelated data normalised above 90 MeV/c. This distribution is obtained by combining the primary pions of one charm event with D mesons from all the other charm events, excluding those that

contribute to the D^* peak of fig. 1. The D^* signal, 18 events above a background of 17, is clearly visible at low p_T. As expected, the same technique, applied to the $D^{\pm}\pi^{\pm}$ and $D^{\pm}\pi^{\mp}$ systems, does not show any excess of events in the low p_T region. This result (18 D^* in a D^o sample of 60) is in good agreement with that already noted.

The second method, applied only to the V2 sample of D^o decays, uses the small difference between D^* and D^o masses. The invariant mass $M(K\pi)$ is computed after making K and π mass assignments either according to particle identification information if available or by accepting both combinations ($K^+\pi^-/K^-\pi^+$). The three-body invariant masses, $M(K\pi\pi)$, are obtained by combining the V2 with all primary vertex charged tracks in turn, assumed to be pions, the quantity $\Delta M = M(K\pi\pi) - M(K\pi)$ is computed for each combination and for the reasons noted above only the minimum value of ΔM is used for each decay. From a sample of 45 V2 decays, with both tracks reconstructed in the spectrometer we obtain the ΔM spectrum shown in fig. 2(b). A Monte-Carlo simulation shows that ΔM is sharply peaked around the value of 145 MeV/c^2 expected for the decay chain $D^* \to D^o\pi$; $D^o \to K\pi...$, even for D^o decays involving undetected neutral particles.

The dashed curve normalized above 200 MeV, is the background predicted by a Monte-Carlo simulation taking into account the charged track reconstruction efficiency and the selection procedure. A similar background is obtained from the uncorrelated data. A signal of 12 events above a background of 5 is clearly seen in the region below 200 MeV. The width of the peak is well reproduced by the Monte-Carlo simulation, folded with our experimental errors, as shown by the solid line in fig. 2(b). This 12 D^* event signal from a total D^o sample of 45 is also in good agreement with the result already given.

To search for D^{*o} we have investigated the two possible decay modes $D^{*o} \to D^o\gamma$ and $D^{*o} \to D^o\pi^o$.

The channel $D^{*o} \to D^o\gamma$ which has the larger acceptance in our apparatus, has a severe background subtraction problem due to the presence of low energy gammas coming from primary or secondary π^o/η decays which are detected as single photons in our gamma detectors.

In spite of the smaller acceptance for the π^o, the situation is more favourable for the channel $D^{*o} \to D^o\pi^o$: because (a) the D^* signal is on the edge of the available phase space, and (b) the presence of a π^o signal, with the additional constraint that the energy of both gammas be greater than 1 GeV, significantly reduces the background.

From the sample of 35 kinematically constrained D^o decays, (14 V4 and 21 V2), we have excluded the 10 contributing to the $D^{*\pm}$ signal. Furthermore another 10 are excluded since they do not have any associated π^o production. In fig. 3 (open histogram) we show the spectrum of the smallest $M(D^o\pi^o)$ for each of the remaining 15 D^o. A peak at low mass value is clearly present, with a width compatible with our mass resolution in the D^* region of 30 MeV FWHM. The poorer mass resolution for the $D^o\pi^o$ system is explained by the much larger errors effecting the π^o energy reconstruction compared to the charged track momentum determination. To estimate the background level below the D^{*o} peak we have used the technique already mentioned of combining each π^o of a charm event with all the other D^o present in the other events of our sample. The resulting histogram, normalized in the mass region $M(D^o\pi^o) > 2.040$ GeV, is shown as a shaded area in fig. 3. We estimate a signal of 7 events over a background of 1.

To compute the total and differential D^* cross section we have used the results based on the 57 reconstructed D decays. Losses due to track reconstruction and visibility are accounted for by using the weights described in [2]. The pion from the $D^{*\pm} \to D^o\pi^\pm$ decay produced at positive x_F has a reconstruction efficiency of 95%. It is in fact kinematically constrained to follow the D^o direction with a momentum greater than 2 GeV/c, for which our spectrometer has almost full acceptance.

The ratio R_1 of $D^{*\pm}$ decaying into $D^0\pi^\pm$ to the total number of $D^0/\bar{D}^0$ is:

$$R_1 = \frac{\sigma(D^{*\pm} \to D^0\pi^\pm)}{\sigma(D^0)} = 0.24\ ^{+0.09}_{-0.06} \quad \text{at} \quad x_F > 0 \ .$$

Using our measured inclusive cross section [2] $\sigma(D^0) = 10.1 \pm 2.2$ μb and the known branching ratio for $D^{*+} \to D^0\pi^+$ [6] of (49 ± 8)% we obtain

$$\sigma(D^{*\pm},\ x_F > 0) = (5.0\ ^{+2.3}_{-1.8})\ \mu b.$$

With this cross section we expect to observe a total of 3 D^* events in the decay channel $D^\pm\pi^0$. Experimentally we find 2 events in the D^* region. Our reduced sensitivity for this channel compared to the $D^0\pi^\pm$ is due to the smaller branching ratio (34 ± 7)% and to the smaller acceptance for π^0.

The same procedure has been applied to the neutral D^* decay. The π^0 from D^* decay at $x_F > 0$ has a reconstruction efficiency of (50 ± 7)%, where the error originates in the uncertainty in the D^* x_F distribution. The ratio R_2 of D^{*0}, decaying into $D^0\pi^0$, to the total number of D^0 in the region $x_F > 0$ is found to be:

$$R_2 = \frac{\sigma(D^{*0} \to D^0\pi^0)}{\sigma(D^0)} = 0.40 \pm 0.13 \ .$$

Using the known branching ratio [6] for $D^{*0} \to D^0\pi^0$ of (54 ± 9)% we obtain for the inclusive cross section:

$$\sigma(D^{*0},\ x_F > 0) = (7.3 \pm 2.9)\mu b.$$

From the above data, we can separate the production of D meson through D^* from direct production. The ratios of indirect (through D^*) to direct production in the forward x_F region are for D^0 and $D^\pm$, respectively:

$$\frac{D^0 \text{ from } D^*}{\text{all } D^0} = \frac{\sigma(D^{*\pm} \to D^0\pi^\pm) + \sigma(D^{*0})}{\sigma(D^0)} = R_1 + \frac{R_2}{BR(D^{*0} \to D^0\pi^0)}$$

$$= 0.98 \pm 0.28;$$

$$\frac{D^{\pm} \text{ from } D^{*}}{\text{all } D^{\pm}} = \frac{\sigma(D^{*\pm} \to D^{\pm}\pi^{o}) + \sigma(D^{*\pm} \to D^{\pm}\gamma)}{\sigma(D^{\pm})} = \frac{\sigma(D^{o})}{\sigma(D^{\pm})} \times \frac{R_{1} \cdot [1-BR(D^{*\pm} \to D^{o}\pi^{\pm})]}{BR(D^{*\pm} \to D^{o}\pi^{\pm})}$$

$$= 0.44 \ ^{+0.25}_{-0.21}$$

where we have used our published value for the $D^{\pm}$ cross section at $x_F > 0$, $\sigma(D^{\pm}) = (5.7 \pm 1.5)\mu b$ [4].

While the D^{o} cross section appears to be saturated by D^{*} production, the $D^{\pm}$ mesons seem to be produced by two distinct mechanisms, although the statistical significance is only at the 2 standard deviation level.

We now consider the production properties of the $D^{*}(2010)$ using the kinematically fitted sample. We have checked, using a Monte-Carlo simulation, that the bias on the x_F and p_T distributions, introduced by the selection procedure, is negligible with respect to the statistical errors.

Fig. 4(a) shows the differential cross section $d\sigma/dp_T^2$ for the $D^{*\pm}$. Parametrizing the experimental distribution with the usual exponential function $\exp(-bp_T^2)$ we get the best fit with

$$b = 0.9 \pm 0.4 \ (GeV/c)^{-2}$$

not significantly different from the value obtained from our total D sample, $b = 1.18 \ ^{+0.18}_{-0.16} \ (GeV/c)^{-2}$ [5] (full line in fig. 4(a)).

Fig. 5(a) shows the x_F distribution for the $D^{*\pm}$. A maximum likelihood fit with the usual form $d\sigma/dx_F \ \alpha(1 - |x_F|)^{n}$ gives

$$n = 4.3 \ ^{+1.8}_{-1.5} \ .$$

The fit is shown as a full line in fig. 5(a). This result may be compared with the value $n = 2.2 \ ^{+1.0}_{-0.9}$ obtained for the D^{+}, D^{-} sample [2]. These values are consistent with those reported by Bailey et al. [1] and taken together the two results suggest that $D^{*\pm}$ may be more centrally produced than $D^{\pm}$. In addition, we have analyzed the full sample of 48 fitted D^{o} decays, to search for D^{*} at large x_F. Of the 17 $D^{*\pm}$ candidates globally obtained in this way, none have $x_F > 0.5$, while 3,

out of the 23 $D^{\pm}$, not originating from a D^{*}, have large x_F values ($x_F > 0.5$), which supports the above suggestion. The difference between the $D^{*\pm}$ sample and the $D^{\pm}$ sample or the leading component D^{-}, D^{o} (for which $n = 1.8^{+0.6}_{-0.5}$ [5]) becomes even more significant if D from D^{*} decays were removed from these last two samples. Consistent with central production, we do not observe a difference in the number of D^{*-} (4 events) compared to the number of D^{*+} (6 events).

Figs 4(b) and 5(b) show the p_T^2 and x_F distributions for the D^{*o} sample. The large errors due to the poor π^o acceptance, do not justify quantitative fits of these distributions. The distributions are compatible with those obtained for the charged D^{*}, as is shown by the dashed curves which display the results of the previous fits.

We note that a simple first order QCD calculation (for example, the broken lines of figs 4(a) and 5(a) show the predictions of ref. [7]) is sufficient to describe the main features of our data.

In conclusion our data indicate that:

(a) D^{*} production dominates the total charm D-meson production and, in particular, saturates D^{o} production.

(b) The differential cross section $d\sigma/dx_F$ for D^{*} production can be described by $\alpha(1 - |x_F|)^4$, without a significant non-central component.

(c) The p_T^2 distribution of the D^{*} agrees with that of the D reported in our inclusive D study [4].

Acknowledgements

We would like to acknowledge the hardware specialists of the bubble chamber crew and the SPS, the painstaking work of the scanning staff at the collaborating laboratories for their contribution to the data selection and the organisational and typing work of Miss M. King. Finally, we would like to thank the various funding agencies of our collaboration for making this work possible.

REFERENCES

[1] R. Bailey et al., Phys. Lett. 132B (1983) 237.

[2] M. Aguilar-Benitez et al., Phys. Lett. 146B (1984) 266;
M. Aguilar-Benitez et al., to be published in Zeitsch. für Phys. C.

[3] M. Aguilar-Benitez et al., Phys. Lett. 123B (1983) 98.

[4] M. Aguilar-Benitez et al., Phys. Lett. 161B (1985) 401.

[5] W.W.M. Allison et al., Nucl. Instr. and Methods 224 (1984) 396.

[6] Errata for the 1984 edition of the Review of Particles Properties, Rev. Mod. Phys. 56 (1984) 523.

[7] R. Odorico, IFNB 85/2 (1985) Bologna University preprint, to be published in Phys. Rev. D.
R. Odorico, Nucl. Phys. B209 (1982) 77.

FIGURE CAPTIONS

Fig. 1 The $D^{o}\pi^{\pm}$ effective mass spectra from kinematically constrained D^{o}'s (open histogram) with background estimations given by the shaded histogram and broken line. The solid line is the expected D^{*} signal folded with our effective mass resolution.

Fig. 2 (a) The $\pi^{\pm}$ transverse momentum distributions with respect to the line-of-flight of the D^{o} (open histogram) with a background estimation given by the shaded histogram.

(b) Invariant mass difference between the $K\pi\pi$ and the $K\pi$ systems for the V2 sample. The dashed line shows the Monte-Carlo background estimation on which is superimposed a peak at low mass that corresponds, in size and width, to the expected D^{*} contribution.

Fig. 3 The $D^{o}\pi^{o}$ effective mass spectrum (open histogram) with a background estimation (shaded histogram).

Fig. 4 (a) The production p_T^2 distribution of the $D^{*\pm}$ sample. The full line shows the result of the fit explained in the text. The broken line shows the predictions of the QCD calculation of ref. [7].

(b) The production p_T^2 distribution of the D^{*o} sample. The broken line reproduces the result of the fit obtained for the $D^{*\pm}$ sample.

Fig. 5 (a) the production x_F distribution for the $D^{*\pm}$ sample. The full line shows the result of the fit explained in the text. The broken line shows the predictions of the QCD calculation.

(b) The production x_F distribution for the D^{*o} sample. The broken line reproduces the result of the fit obtained for the $D^{*\pm}$ sample.

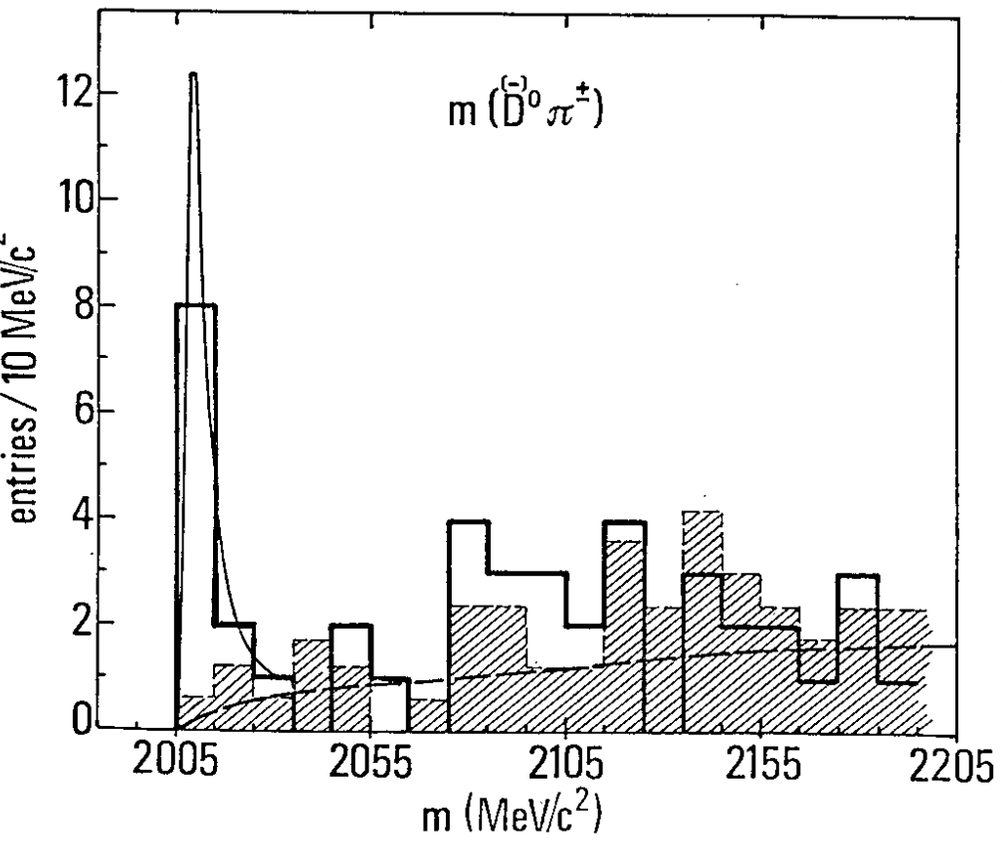
m ($\bar{D}^0\pi^\pm$)
entries / 10 MeV/c^2
0
2
4
6
8
10
12
2005
2055
2105
2155
2205
m (MeV/c^2)

fig. 1

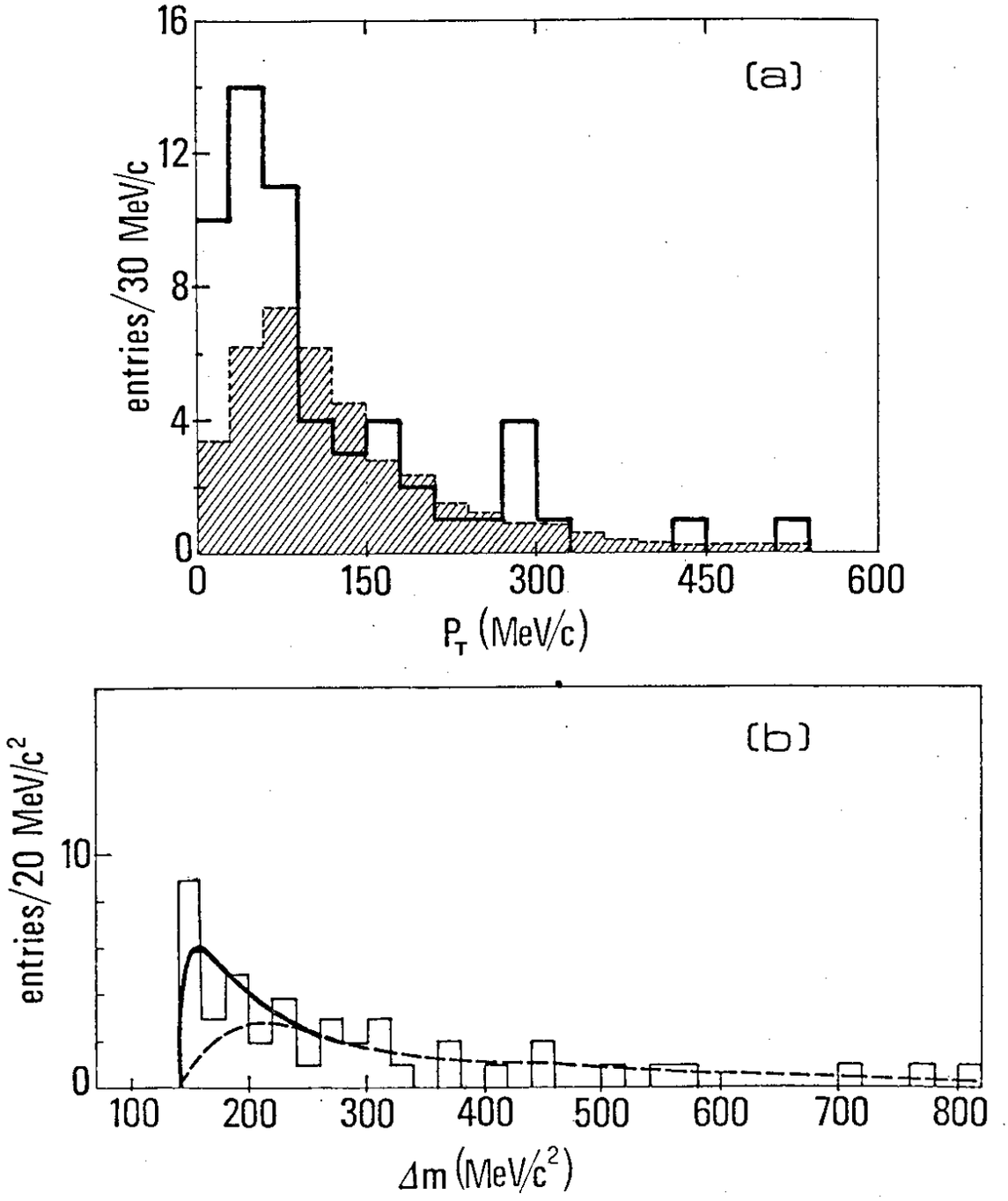
(a)
entries/30 MeV/c
16
12
8
4
0
0
150
300
450
600
P_T (MeV/c)
(b)
entries/20 MeV/c^2
10
0
100
200
300
400
500
600
700
800
Δm (MeV/c^2)

fig. 2

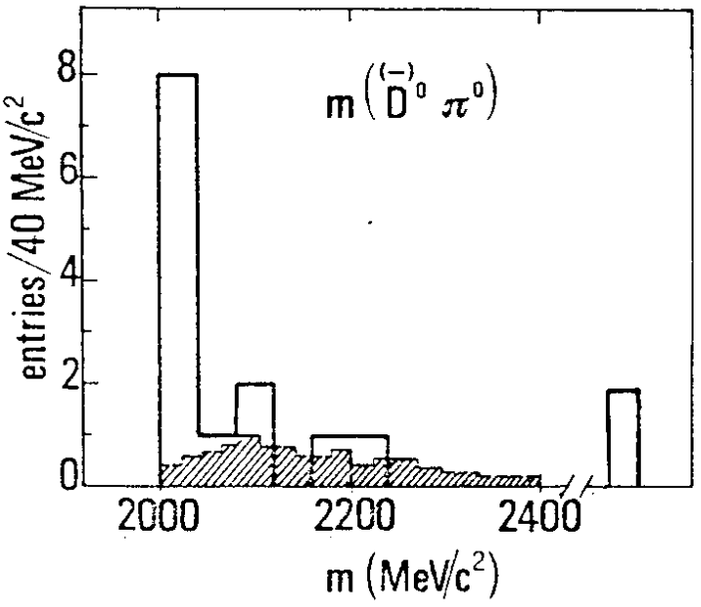

fig. 3

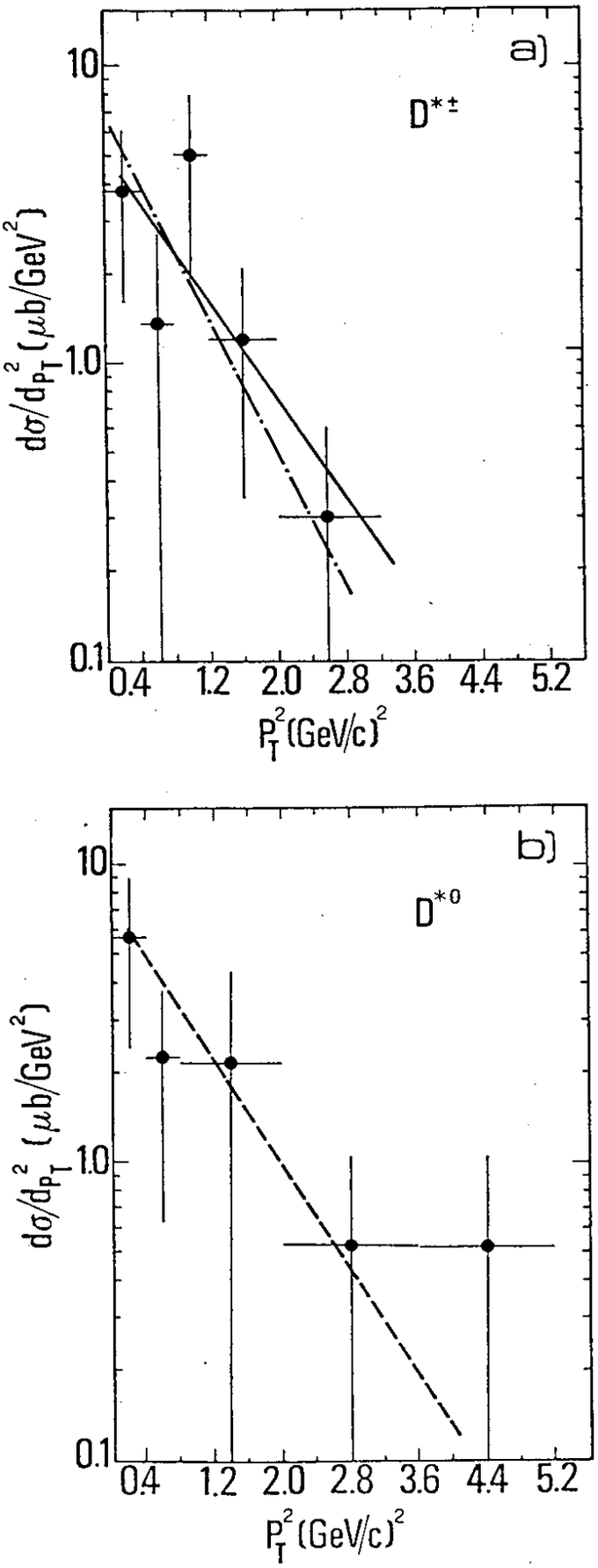
a)
$D^{*\pm}$
10
1.0
0.1
$d\sigma/dp_T^2$ (μb/GeV^2)
0.4 1.2 2.0 2.8 3.6 4.4 5.2
P_T^2 (GeV/c)^2
b)
D^{*0}
10
1.0
0.1
$d\sigma/dp_T^2$ (μb/GeV^2)
0.4 1.2 2.0 2.8 3.6 4.4 5.2
P_T^2 (GeV/c)^2

fig. 4

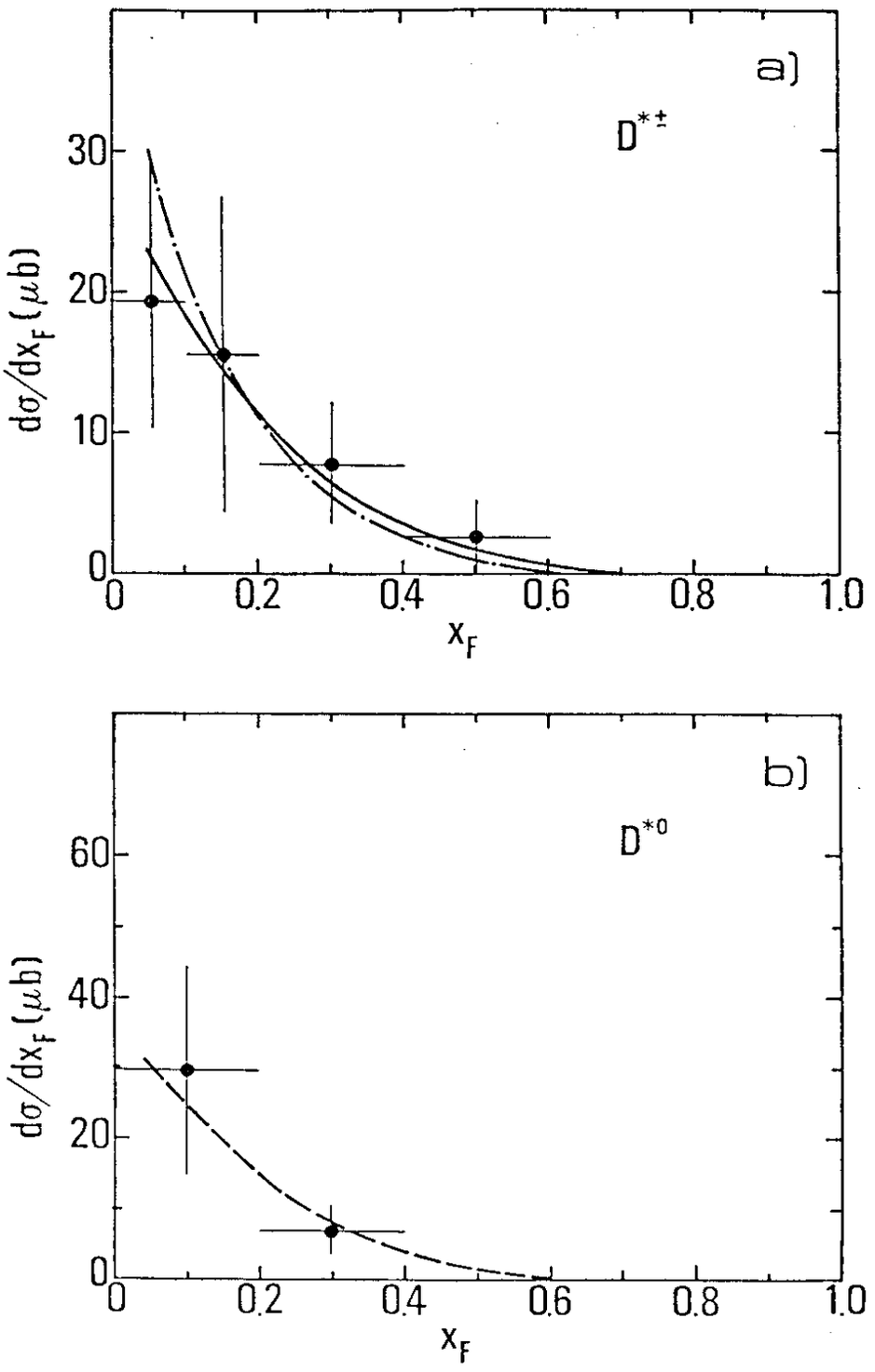
a)
$D^{*\pm}$
30
20
10
0
$d\sigma/dx_F$ (μb)
0
0.2
0.4
0.6
0.8
1.0
x_F
b)
D^{*0}
60
40
20
0
$d\sigma/dx_F$ (μb)
0
0.2
0.4
0.6
0.8
1.0
x_F

fig.5